# BEND INSTALLATION EFFECTS ON THE CORRECTION FACTOR OF SINGLE PATH ULTRASONIC FLOW METERS

**Ramon S. Martins*** **and Rogério Ramos**

*LFTC/PPGEM, Department of Mechanical Engineering, Universidade Federal do Espírito Santo, Avenida Fernando Ferrari, 514, Goiabeiras, 29075-910, Vitória, ES, Brazil, http://www.ufes.br/ppgem*

**Keywords:** ultrasonic flow meter, installation effects, correction factor, computational fluid dynamics.

**Abstract.** Oil and gas industry requires accurate flow measurement since they are stated by law. Though, such industry fields usually deal with installation effects on the quality of flow profile due to pipe connectors, for instance. Hence, flow disturbances occur and measurement accuracy may be committed. On the other hand, single path ultrasonic flow measurement technology depends on being installed at a tube section where fully developed flow is established. The paper presents an evaluation of bend effects, installed upstream to the flow meter, on the correction factor ($k$ factor) of such devices. The flow field has been obtained via computational fluid dynamics (CFD) and the correction factor has been calculated by numerical integration of the velocity profile at the metering section. Typical pipe curves configuration (single bend and double bend out-of-plane) have been considered. The $k$–$\varepsilon$ turbulence model has been used to all simulations. Reynolds numbers from 1x10$^5$ to 2x10$^6$, transducer installation angles of 0, 30, 45, 60 and 90$^o$ and distances of 5, 10, 15, 20, 40, 60 and 80$D$ after curve have been tested and previous results are graphically shown and commented.

*e-mail address:* ramonsmartins@gmail.com

## 1 INTRODUCTION

Flow meters calibration represents an important issue to oil and gas industry, where accurate flow measurements are required and national regulations describe the proceedings for operational and custody metering. These documents, such as AGA (2007) and ANP/INMETRO (2000), point out ultrasonic flow meters (UFM) as a suitable technology for oil and gas metering. Still, the conditions for accurate flow measurements may be not reliable due to several installation obstacles, such as bends, valves and diameter step changes. In many cases, due to available space, such obstacles are close to the metering section causing flow disturbances. Since the majority of flow meters depends on fully developed flow condition at these locations, the flow metering is thus compromised in such situations.

Scientific and technological community has been evaluating flow disturbances patterns and consequences as well as methods to diminish flow measurement errors and uncertainties. Ruppel and Peters (2004) and Mickan et al. (1997) identify downstream flow patterns of typical pipe installation by means of experiments. Hilgenstock and Ernst (1996) compare computational fluid dynamics (CFD) results and experiments, pointing numerical simulations as an interesting tool for meters calibration and diagnostic. Moore et al. (2000) evaluate several mathematical models for disturbed profiles and present an analytical sensitivity study of UFM for some configurations. Holm et al. (1995) proposed the calculation of a numerical $k$ factor in order to evaluate various installation effects on UFM. Ferreira (2010) presents a modern numerical approach about disturbed flows and numerical $k$ factor calculation. Hilgenstock and Ernst (1996); Ruppel and Peters (2004); Moore et al. (2000); Ferreira (2010) also explore UFM sensibility to several transducers installation angles ($\theta$).

On the other side, according to their measurement principle, UFM are relatively sensitive to flow profile disturbances and such dependence can be better understood by knowing their basic configuration and operational fundamentals.

UFM are composed, at least, by two ultrasonic transducers transmitting and receiving ultrasonic pulses through the fluid, so composing a single acoustic channel (the so called *sound path*) with a certain inclination ($\alpha$) relative to the pipe axis and with another inclination ($\theta$) relative to the vertical axis ($y$-axis), as shown in Fig. 1.

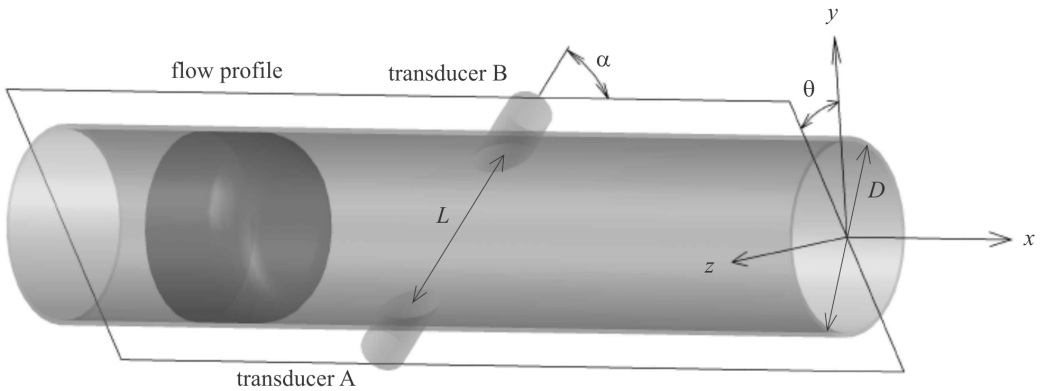


Figure 1: Sound path installation angle.

Transit time UFM detect the time the ultrasonic pulse takes to travel from a transducer to the other. Transit mean velocities are then obtained by dividing the length ($L$) by the measured times. Because there is a flow velocity field, transit time from transducer A to B ($t_{AB}$) is smaller

then transit time from transducer B to A ($t_{BA}$). The transit mean velocities represent the mean velocities of the acoustic pulse along the sound path, downstream and upstream ($\bar{u}_{AB}$ and $\bar{u}_{BA}$, respectively). These velocities are composed by the sound propagation velocity in the fluid ($c$) plus a portion ($\bar{V}_{SP}$) which represents the interference of the flow velocity field in the acoustic signal velocity, as show in Eqs. (1) and (2).

$$\bar{u}_{AB} = \frac{L}{t_{AB}} = c + \bar{V}_{SP} \tag{1}$$

$$\bar{u}_{BA} = \frac{L}{t_{BA}} = c - \bar{V}_{SP} \tag{2}$$

The unknowns $\bar{V}_{SP}$ and $c$ can be found by solving the algebraic system of Eqs. (1) and (2) and the result is shown in Eqs. (3) and (4).

$$c = \frac{D}{2\sin\alpha}\left(\frac{t_{AB} + t_{BA}}{t_{AB}t_{BA}}\right) \tag{3}$$

$$\bar{V}_{SP} = \frac{D}{\sin 2\alpha}\left(\frac{t_{AB} - t_{BA}}{t_{AB}t_{BA}}\right) \tag{4}$$

Due to their measurement principle, UFM calculate $c$ and $\bar{V}_{SP}$. Nevertheless the flow cross sectional mean velocity ($\bar{u}_m$) is useful on volumetric flow rate ($Q$) calculation. May $A$ be the pipe cross sectional area and $\bar{u}_m$ the uniform flow velocity perpendicular to $A$, $Q$ may be then obtained by Eq. (5).

$$Q = \bar{u}_m A \tag{5}$$

UFM use a correction factor ($k$), also called profile factor (Köchner et al., 1996) or hydrodynamic factor (Moore et al., 2000) to obtain $\bar{u}_m$ from $\bar{V}_{SP}$ (Eq. (6)). (Carlander and Delsing, 2000; Mylvaganam, 1989)

$$\bar{u}_m = k\bar{V}_{SP} \tag{6}$$

The volumetric flow rate ($Q$) is finally obtained by Eq. (7).

$$Q = k\bar{V}_{SP}A \tag{7}$$

This $k$ factor is an input parameter to UFM and impacts directly on the flow rate reading, as shown in Eq. (7). In order to obtain it AGA (2007) and ABNT (2010) indicate the classical profile of Nikuradse (1966) for turbulent fully developed flows. Since it depends on the flow profile, there is a relationship between $k$ factor and Reynolds number (AGA, 2007; ABNT, 2010; Nikuradse, 1966; Schlichting, 1968), based in fully developed flow condition. Because UFM expect fully developed flow, the scientific community tries to better understand how the absence of this condition (i.e. the presence of disturbed flows) may interfere in the flow rate measurement quality (Holm et al., 1995; Hilgenstock and Ernst, 1996; Mickan et al., 1997; Moore et al., 2000; Ruppel and Peters, 2004; Ferreira, 2010).

This paper presents a comparative analysis between numerical $k$ factors for disturbed and fully developed cases. Two pipe configurations have been tested and both numerical and analytical fully developed $k$ factors are considered. The analysis explores variation of UFM distance from pipe bend, UFM transducers installation angle ($\theta$) and Reynolds number.

## 2 MATHEMATICAL MODEL AND NUMERICAL SIMULATION PARAMETERS

This section presents the governing equations used to mathematical modeling, the boundary conditions, geometry configurations, meshes, the numerical method used to obtain all follow results and the calculation of the numerical correction factor.

### 2.1 Conservation equations

Considering stationary flow, fluid incompressibility and constant viscosity conditions, the turbulent flow may be predicted by the mass and the momentum conservation equations. These equations need statistical treatment so that time depend fluctuations of the turbulent phenomenon can be considered (Tennekes and Lumley, 1972). Once these statistical method is applied, mass and momentum conservation equation may be given in index notation by Eqs. (8) and (9), respectively.

$$\frac{\partial \rho u_i}{\partial x_i} = 0 \tag{8}$$

$$\rho \frac{\partial (\bar{u}_i \bar{u}_j)}{\partial x_i} = -\frac{\partial \bar{p}}{\partial x_j} + \frac{\partial}{\partial x_i}\left[(\mu + \mu_T)\left(\frac{\partial \bar{u}_i}{\partial x_j} + \frac{\partial \bar{u}_j}{\partial x_i}\right)\right] \tag{9}$$

Where $\rho$ is the fluid density, $u_i$ is the velocity component in direction $i$, $\bar{u}_i$ is the turbulent mean velocity in direction $i$, $\bar{p}$ is the turbulent mean pressure, $\mu$ is the dynamic viscosity and $\mu_T$ is the turbulent viscosity, given by the turbulence model.

### 2.2 Turbulence modeling

The momentum equation considering turbulence needs additional equations to be solved. These equations come from the turbulence model. In this paper the standard $k$–$\varepsilon$ model has been used, as well as the Boussinesq hypothesis, which considerate the turbulent viscosity ($\mu_T$) for the relation between the Reynolds stresses tensor and the turbulent mean velocity, as shown in Eq. (10). (Schlichting, 1968)

$$\tau_{Tij} = \mu_T \left(\frac{\partial \bar{u}_i}{\partial x_j} + \frac{\partial \bar{u}_j}{\partial x_i}\right) \tag{10}$$

Where $\tau_{Tij}$ is the Reynolds stresses tensor. Two extra transport equations must be solved in order to obtain $\mu_T$. Transport equations for $k$ (turbulence kinetic energy) and for $\varepsilon$ (turbulence eddy dissipation) are Eqs. (11) and (12), respectively. (Launder and Spalding, 1974)

$$\rho \frac{\partial (\bar{u}_i k)}{\partial x_j} = \frac{\partial}{\partial x_j}\left[\left(\mu + \frac{\mu_T}{\sigma_k}\right)\frac{\partial k}{\partial x_i}\right] + P_k - \rho\varepsilon \tag{11}$$

$$\rho \frac{\partial (\bar{u}_i \varepsilon)}{\partial x_j} = \frac{\partial}{\partial x_j}\left[\left(\mu + \frac{\mu_T}{\sigma_\varepsilon}\right)\frac{\partial \varepsilon}{\partial x_i}\right] + \frac{\varepsilon}{k}\left(C_{\varepsilon 1} P_k - C_{\varepsilon 2}\rho\varepsilon\right) \tag{12}$$

Where $P_k$ is obtained from Eq. (13) and $\sigma_k$ , $\sigma_\varepsilon$, $C_{\varepsilon 1}$ and $C_{\varepsilon 2}$ are constants of the model and their values are presented in Tab. 1.

$$P_k = \mu_T \frac{\partial \bar{u}_i}{\partial x_j}\left(\frac{\partial \bar{u}_i}{\partial x_j} + \frac{\partial \bar{u}_j}{\partial x_i}\right) \tag{13}$$

The turbulent viscosity ($\mu_T$) is finally obtained from Eq. (14).

$$\mu_T = \rho C_\mu \frac{k^2}{\varepsilon} \tag{14}$$

Where $C_\mu$ is a constant of the model and its value is also presented in Tab. 1. (Launder and Spalding, 1974; Versteeg and Malalasekera, 2007)

Table 1: Constants of the standard $k$–$\varepsilon$ model.

| $\sigma_k$ | $\sigma_\varepsilon$ | $C_{\varepsilon 1}$ | $C_{\varepsilon 2}$ | $C_\mu$ |
|---|---|---|---|---|
| 1.0 | 1.3 | 1.44 | 1.92 | 0.09 |

## 2.3 Geometries and meshes

Two typical pipe configurations have been carried out in this paper: single bend and double bend out-of-plane. In both cases internal diameter of 300 mm has been used as well as the 100D (30,000 mm) downstream straight pipe length. Each pipe bend has internal curvature radius of 1.0D and has been positioned downstream of a 2.0D length straight pipe. These geometries are illustrated in Figs. 2 and 3.

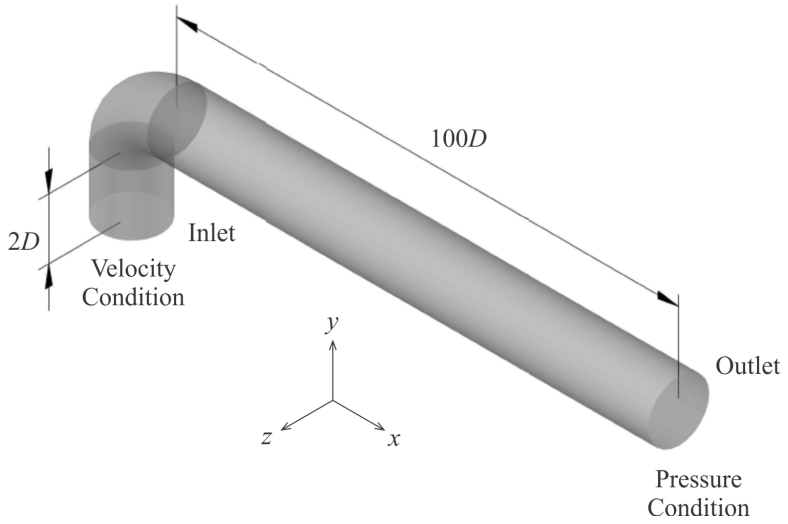


Figure 2: Single bend pipe configuration.

Several hexahedral meshes have been tested. The meshes have been generated by ANSYS ICEM CFD$^{TM}$ with Multiblock technique. The test consisted in doubling the number of mesh nodes and analysing if it still influences some reference parameters. Volumes maximum size and height have been varied in order to generate finer meshes. Figure 4 shows the meshes tested in the single bend case in this paper. Same proceedings have been used in the double bend case. Mesh tests results are better commented in section 3.

## 2.4 Boundary conditions and fluid model

Boundary conditions are also necessary to solve the governing equations system. Here, smooth wall and no slip condition have been considered for pipe wall. Inlet condition has been set as normal uniform velocity profile so that desired Reynolds numbers were achieved.

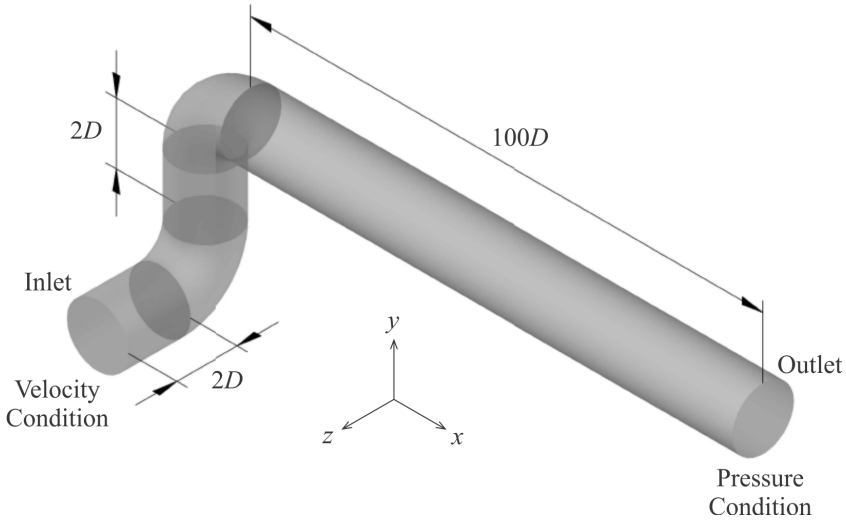


Figure 3: Double bend pipe configuration.

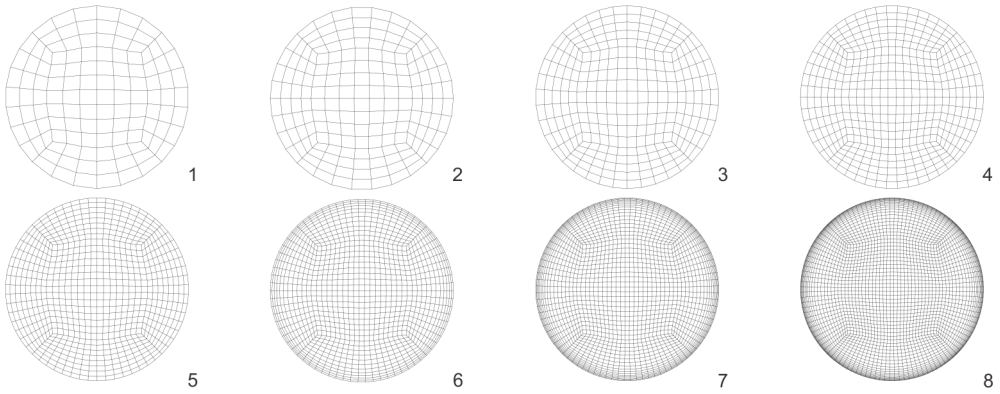


Figure 4: Hexahedral meshes used for numerical solution.

Turbulence parameters ($k$ and $\varepsilon$) at the inlet have been set according to the turbulence intensity ($I$), defined by Eq. (15).

$$I = \frac{u'}{\bar{u}} \tag{15}$$

Where $u'$ is the root mean square of the turbulent velocity fluctuations and $\bar{u}$ is the mean velocity.

In the absence of any experimental data, turbulent intensity is set as medium ($3.7\%$), i.e., $I = 0.037$, as suggested by Ansys, Inc. (2010a). Therefore, inlet boundary conditions may be expressed by the set of Eq. (16), as follows.

$$u_{inlet} = \frac{\mu Re}{\rho D}; v_{inlet} = 0; w_{inlet} = 0; k_{inlet} = \frac{3}{2} I^2 \bar{u}^2; \varepsilon_{inlet} = \rho C_\mu \frac{k^2}{\mu_T} \tag{16}$$

Where the relation $\mu_T = 1000 I \mu$ is used. (Ansys, Inc., 2010a)

Average static pressure (in the same value of reference pressure, i.e., 1 atm) has been set as

overall outlet condition. Such condition is mathematically represented by Eq. (17).

$$\bar{p}_{outlet} = 1atm = \frac{1}{A}\int_A p_{ip,outlet}\,\mathrm{d}A \tag{17}$$

Where $p_{ip,outlet}$ is the pressure at each integration point over the outlet.

By modeling the fluid, air at 25$^o$C has been considered in all cases. Table 2 resumes such fluid input parameters.

Table 2: Synthesis of fluid parameters.

| **Fluid** | Air at 25$^o$C |
|---|---|
| **Density ($\rho$)** | 1.185 kg/m$^3$ |
| **Dynamic Viscosity ($\mu$)** | 1.831x10$^{-5}$ kg/m.s |
| **Reference Pressure** | 1 atm |

### 2.5 Numerical solution

Commercially available CFD code has been used to achieve numerical solution (Ansys, Inc., 2010b). The software uses the Finite Volume Method conjugated with Multigrid accelerated Incomplete Lower Upper factorization technique for solving the discrete governing equations algebraic system. As convergence criteria, the root mean square (RMS) residuals of the linear solution of discrete governing equations are controlled to be smaller than 1x10$^{-8}$ with double precision. The advection scheme chosen was the High Resolution (Ansys, Inc., 2010a). All runs were performed by the 8 machines cluster at Laboratório de Fenômenos de Transporte Computacional (LFTC) of Universidade Federal do Espírito Santo (Ufes). Each PC is equipped with Quad Core processor 2.4 GHz, 4.0 GB memory and 8 MB cache.

### 2.6 Calculation of the $k$ factor

Equation (7) shows that any deviation in the $k$ factor interferes directly the flow rate. In this paper, the $k$ factor is numerically obtained in order to quantify the deviation in the flow rate due to flow disturbances. This numerical approach is based on Holm et al. (1995) suggestion and uses numerical integration to obtain $\bar{V}_{SP}$.

Before any mathematical treatment, it is important to remark the assumptions to this approach. In fact, the sound path is complex, since it depends on acoustics and its interaction with the flow field, as shown by Yeh and Mattingly (1997). It is also known that velocity gradients along the sound path refract it, as specified by Mathias (2010). However, in this paper, linear and non-deformable sound path has been considered. More reasonable treatment of the such relations between the sound path and the flow field is a goal for further work.

AGA (2007) defines the correction factor ($k$), except for the vector approach, as shown in Eq. (18).

$$k = \frac{\bar{u}_m}{\bar{V}_{SP}} = \frac{\frac{1}{A}\int_A \vec{u}(x,y,z)\cdot \mathrm{d}\vec{A}}{\frac{1}{L}\int_L \vec{u}(x,y,z)\cdot \mathrm{d}\vec{L}} \tag{18}$$

The Reynolds number is used to obtain $\bar{u}_m$ as shown in Eq. (19).

$$\bar{u}_m = \frac{\mu Re}{\rho D} \tag{19}$$

According to the given definition in Eq. (18) above, $\bar{V}_{SP}$ may be mathematically interpreted as the velocity projections' mean value over and in the direction of the sound path. Using the coordinate system and angles shown in Fig. 1 the projection of any three dimensional velocity vector may be represented as a function of its components $u$, $v$ and $w$ by Eq. (20).

$$\bar{V}_{SP} = \frac{1}{L}\left(\int_L u\,\mathrm{d}L\cos\alpha + \int_L v\,\mathrm{d}L\sin\alpha\cos\theta + \int_L w\,\mathrm{d}L\sin\alpha\sin\theta\right) \tag{20}$$

The Trapeze Rule (Filho, 2007) has been applied in order to solve the integrals above. The general formulation for numerical integration of $\bar{V}_{SP}$ gets the form represented in Eq. (21).

$$\bar{V}_{SP} = \frac{1}{L}\sum_{p=2}^{N+1}\left[\frac{(u_p + u_{p-1})}{2}\cos\alpha + \frac{(v_p + v_{p-1})}{2}\sin\alpha\cos\theta + \frac{(w_p + w_{p-1})}{2}\sin\alpha\sin\theta\right]\Delta L \tag{21}$$

Where $N$ is the number of integration points, the subscript $p$ indicates the value of a velocity component at the $p$-th integration point and $\Delta L$ is given by $L_p - L_{p-1}$.

### 2.7 The calculation of *k* factor error

Since the $k$ factor is directly related to the flow rate calculation, it is important to quantify its error due to disturbances. Many authors have evaluated this error, $\Delta k$, (Hilgenstock and Ernst, 1996; Ruppel and Peters, 2004; Ferreira, 2010) as follows in Eq. (22).

$$\Delta k = \frac{k_{dist} - k_{ref}}{k_{ref}} \tag{22}$$

Where $\Delta k$ is the error shift, $k_{dist}$ is the numerical $k$ factor obtained for a disturbed profile and $k_{ref}$ is the reference $k$ factor.

In this paper, two references have been compared: the semi-empirical results of Nikuradse (1966), which is suggested by AGA (2007) and ABNT (2010) as the fully developed turbulent profile; and the numerical results obtained by Martins and Ramos (2011b) for a straight pipe, $80D$ from the entrance for several Reynolds numbers.

## 3 RESULTS AND DISCUSSION

The main results to the mesh test are now presented and commented. Table 3 presents some features of the double bend case, which has presented slower converge compared with the single bend case. It is important to remark that from mesh 2 on, the result of the previous mesh has been set as the initial condition for the current processing.

Reynolds number 1x10$^5$ has been set during the mesh test. Figure 5a shows the $u$ velocity at pipe center along the straight section after the second bend for all tested meshes. Figures 5b, 5c and 5d present non-dimensional velocity components (respectively $u$, $v$ and $w$) along $y$-axis $20D$ after the second bend. Such axis and straight length have been chosen just for example.

Figure 5 indicates that from mesh 6 on, the velocities near the wall have not been influenced by the mesh resolution any more. This behavior is easily noticed in Figs. 5b and 5d. Nevertheless, Figs. 5a and 5c suggest that mesh 6 does not represent well the results of mesh 7. On

Table 3: Computational features for double bend case mesh test.

| Mesh | Nodes | CPU time [min] | Number of processors |
|---|---|---|---|
| 1 | 90,400 | 5 | 31 |
| 2 | 187,016 | 8 | 31 |
| 3 | 363,463 | 13 | 30 |
| 4 | 710,494 | 28 | 30 |
| 5 | 1,476,708 | 47 | 30 |
| 6 | 2,924,394 | 93 | 30 |
| 7 | 5,793,672 | 154 | 30 |
| 8 | 10,629,820 | 280 | 32 |

the other hand, mesh 7 reproduces reasonably mesh 8 for all tested parameters. Thus, mesh 7 has been chosen to run all other double bend cases in this work. Same methodology has been applied to the single bend case. Once its features are quite similar they are not resumed in a table in this paper.

Figure 6 shows $k$ factor calculation for the single bend case, considering variation of installation angle, $\theta$ (0, 30, 45, 60 and 90$^o$), straight pipe length, $x/D$ (5, 10, 15, 20, 40, 60 and 80) and Reynolds number from 1x10$^5$ to 2x10$^6$. As commented in section 2.7, the $k$ factor at $80D$ of a straight pipe has been considered as a fully developed flow profile obtained by Martins and Ramos (2011b) and it is shown in all straight pipe lengths as a reference. The $k$ factor suggested by AGA (2007) and ABNT (2010) is shown as well.

As can be noticed, the $k$ factor obtained at $80D$, considering distinct installation angles, tends to collapse, as expected for a flow profile almost symmetric. For shorter straight pipe lengths, the calculated $k$ factors tend to be greater than fully developed case and vary with the installation angle.

At $5D$, the $k$ factor error (calculated using Eq. (22) presented in section 2.7) for $\theta = 90^o$ reaches the maximum 7.58% when compared to the fully developed case, considering Martins and Ramos (2011b) profile. If the error is calculated based on Nikuradse (1966) profile, its value is 8.74%.

For other straight lengths, the maximum error is reached for $\theta = 0^o$. Such behavior is expected since flow asymmetries are remarkable at this angular position (Hilgenstock and Ernst, 1996; Ruppel and Peters, 2004; Ferreira, 2010). Generally speaking, $k$ factor error tends to reduce from shorter to longer straight lengths, once the flow field tends to the fully developed case.

It is remarkable the behavior of $\Delta k$ for $\theta = 30^o$. For such installation angle, $k$ factor errors vary from 0.01% to 3.12% at all straight lengths for Martins and Ramos (2011b) reference. If Nikuradse (1966) reference is considered, $\Delta k$ varies from 0.12% to 4.11%. For all other installation angles, these variation occurs between 0.01% and 7.58% for Martins and Ramos (2011b) reference and between -0.03% and 8.74% for Nikuradse (1966) profile. Such behavior may indicate new proceedings for installation of ultrasonic flow meters, in order to reduce data reading errors.

On the other hand, Fig. 7 shows the behavior demonstrated by $k$ factor generated by double bend configuration. As observed to the former case, shorter straight lengths generate $k$ factors quite distinct from the fully developed flow.

Although the $k$ factor errors tend to reduce at longer straight lengths, when compared to

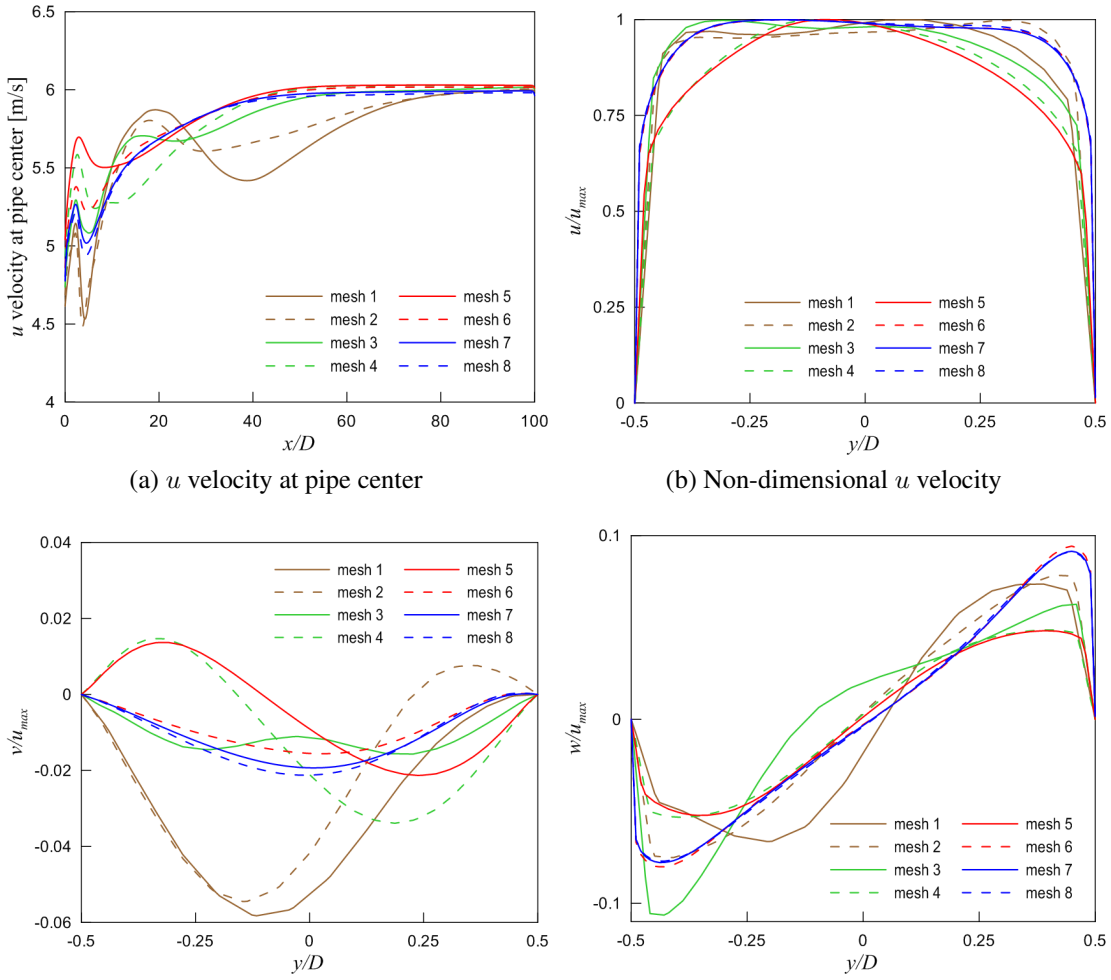


(a) $u$ velocity at pipe center

(b) Non-dimensional $u$ velocity

(c) Non-dimensional $v$ velocity

(d) Non-dimensional $w$ velocity

Figure 5: Mesh test results for Reynolds number 1x10$^5$.

the fully developed case, such reduction is not as well behaved as observed in the single bend configuration. This behavior is consequence of the complex flow effects generated by the pipe bends and may reach 8.77% for $\theta = 30^o$ at $20D$, having Martins and Ramos (2011b) as the reference profile. If Nikuradse (1966) profile is considered, such maximum shift is 9.82% for the same conditions.

Typically, UFM computers obtain the correct $k$ factor by a convergence process which calculates a zero of function. The double bend $k$ factor curves show positive and negative derivatives and inflexion points, which increase computational effort for these purposes. Such behavior may be easily noticed at $20D$.

Such effects tends to reduce at longer straight pipes and it is not completely eliminated even at $80D$, where the errors reaches the maximum of -1.07% for $\theta = 0^o$, considering Martins and Ramos (2011b) profile. If the error is calculated based on Nikuradse (1966) profile, its value is 1.56% for $\theta = 60^o$.

## 4 FINAL REMARKS

Numerical simulations using CFD techniques have been used to calculate the flow field for two typical pipe configurations: single bend and double bend out-of-plane. Numerical inte-

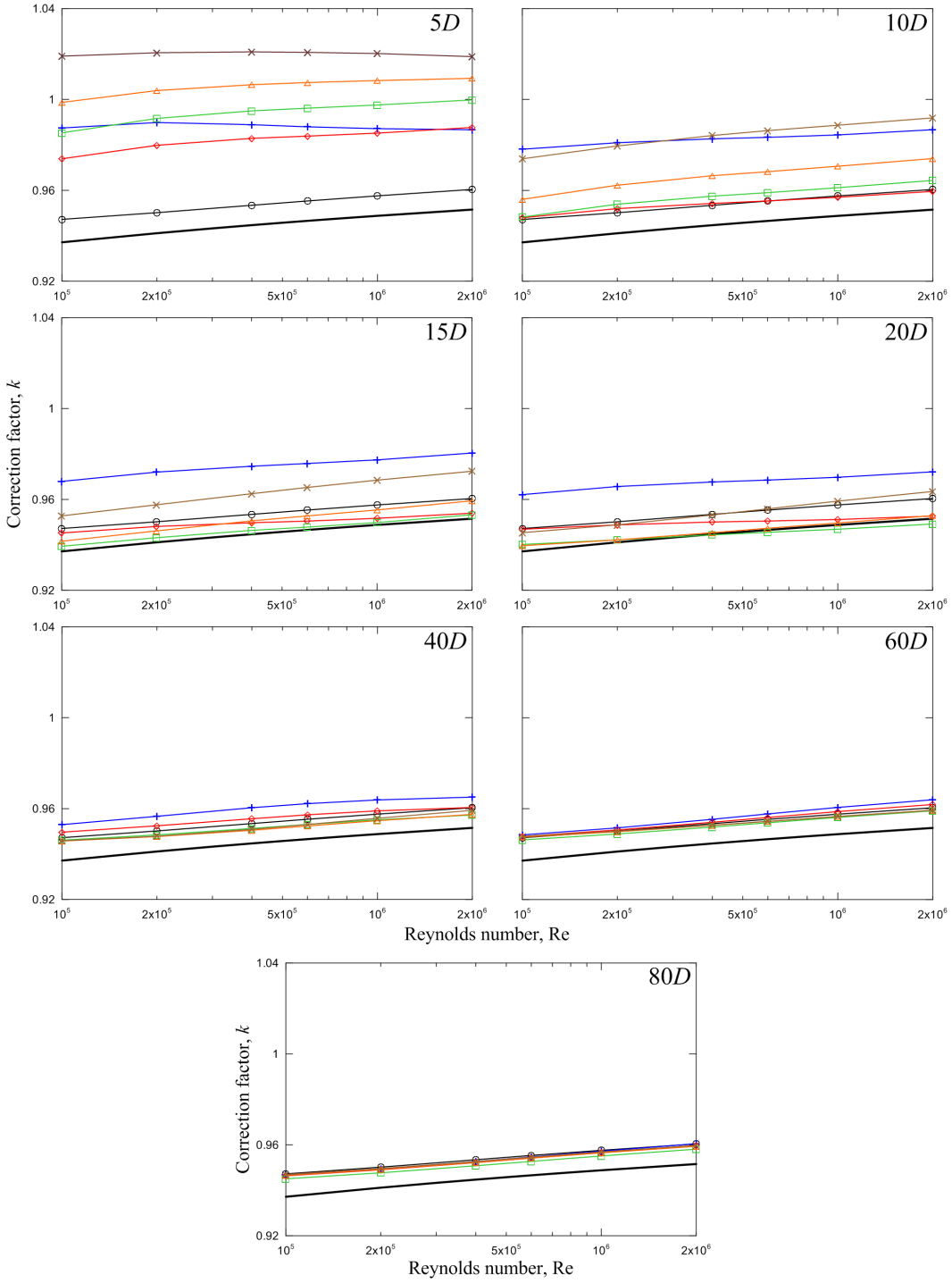


Figure 6: Correction factor ($k$) *versus* Reynolds number (Re) for several distances from the single bend ($x$) and installation angles ($\theta$): (+) $\theta = 0^o$, (◇) $\theta = 30^o$, (□) $\theta = 45^o$, (△) $\theta = 60^o$, (×) $\theta = 90^o$, (○) numerical fully developed case (Martins and Ramos, 2011b) and (—) analytical fully developed based on Nikuradse (1966) profile.

gration has allowed the calculation of numerical correction factors for UFM. The results for several Reynolds numbers, transducers installation angles and straight pipe lengths have been compared with two references (Martins and Ramos, 2011b; Nikuradse, 1966).

Disturbed flows have presented errors of several magnitudes according to the varied parameters. Such error shifts have tended to be shorter when Martins and Ramos (2011b) $k$ factors

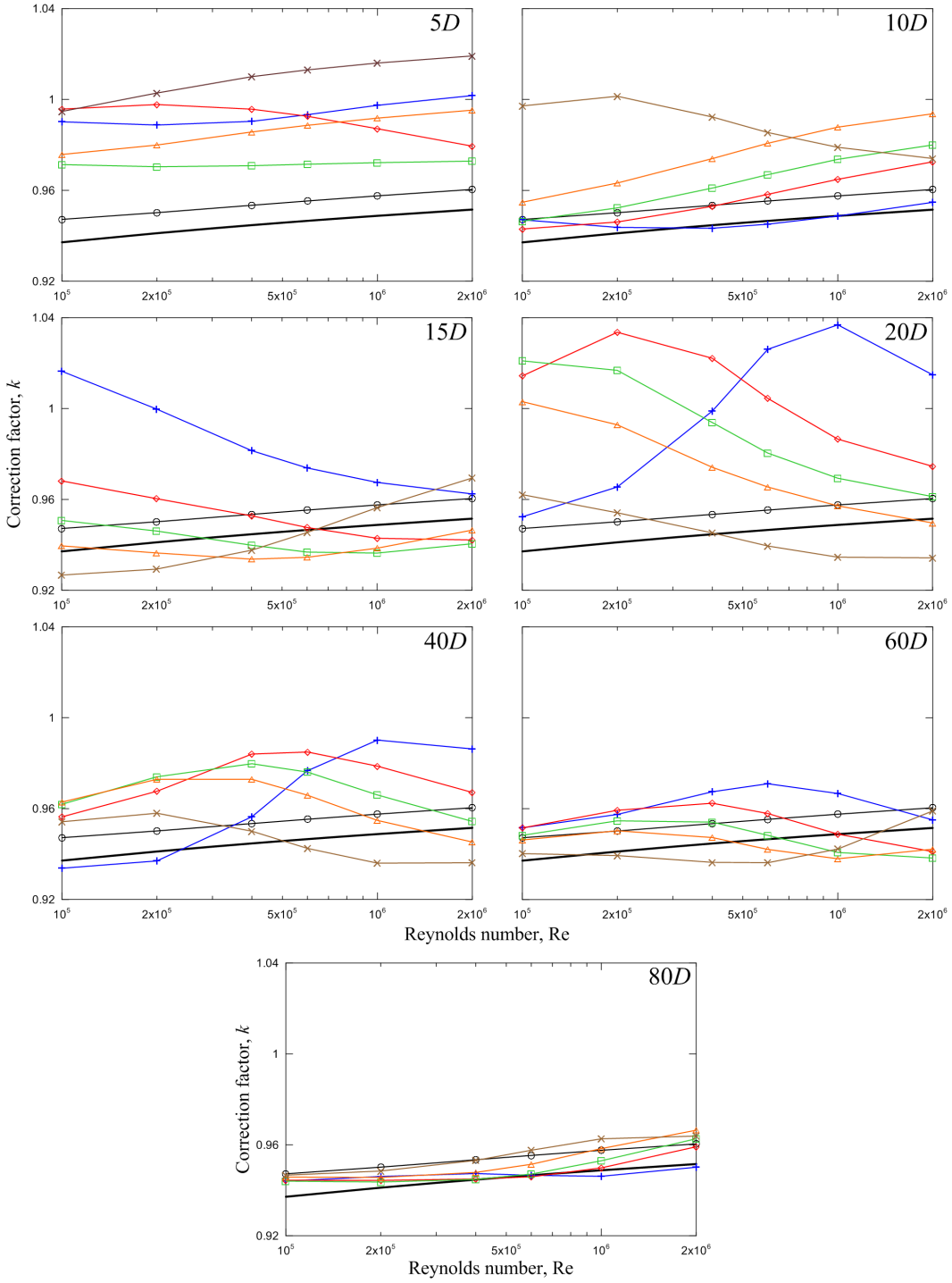


Figure 7: Correction factor ($k$) *versus* Reynolds number (Re) for several distances from the double bend ($x$) and installation angles ($\theta$): (+) $\theta = 0^o$, (◇) $\theta = 30^o$, (□) $\theta = 45^o$, (△) $\theta = 60^o$, (×) $\theta = 90^o$, (○) numerical fully developed case (Martins and Ramos, 2011b) and (—) analytical fully developed based on Nikuradse (1966) profile.

have been considered instead of Nikuradse (1966) $k$ factors as the fully developed reference. Since Nikuradse (1966) profile is suggested by AGA (2007) and ABNT (2010), the present results may indicate, at least, a revision of such documents.

UFM have shown reasonable sensibility to transducer installation angle, which confirms the results of Hilgenstock and Ernst (1996), Ruppel and Peters (2004), Moore et al. (2000) and

Ferreira (2010). It is important to remark the results for $30^o$ for the single bend case. Such angle have presented shorter error shifts at all straight pipe lengths. A reconsideration of the UFM installation proceedings is suggested aiming error reductions.

The present results also suggest that the developed flow condition is almost achieved at $80D$ downstream of a single bend, as commented by Martins and Ramos (2011a). But $k$ factor error shift still reaches the maximum of $1.05\%$ or $0.28\%$ at $80D$ when compared to Martins and Ramos (2011b) and Nikuradse (1966), respectively.

Double bend cases have presented more complex results, which may be explained by the swirl effect downstream of such pipe configuration. The difficulty to handle with convergence processes in order to calculate the correct $k$ factor has been commented, since the curves of $k$ *versus* $Re$ have presented derivative sign changes.

Finally, since there are more appropriate turbulence models to take into account flows with vortex and swirl effects (Versteeg and Malalasekera, 2007), the use of Reynolds stresses models, or even LES, is now commented as a goal for future research work. The comparison between numerical and experimental swirl effects by means of tangential velocity profiles as well as the relations between acoustics and flow dynamics are goal for further work as well.

***Acknowledgments***

The authors would like to express their acknowledgements to Programa de Recursos Humanos – PRH-29b of Universidade Federal do Espírito Santo by Agência Nacional de Petróleo, Gás Natural e Biocombustíveis – ANP for financing this project and for the grant, as well as to Laboratório de Fenômenos de Transporte Computacional – LFTC/Ufes for the use of its computational facilities.

## REFERENCES

ABNT. ABNT NBR 15855:2010 - Medição de gás por medidores do tipo ultra-sônicos multitrajetórias. Norma brasileira, Associação Brasileira de Normas Técnicas, Rio de Janeiro, Brazil, 2010.

AGA. Measurement of gas by multipath ultrasonic meters. Report No. 9, American Gas Association, Washington, DC, USA, 2007.

ANP/INMETRO. Portaria Conjunta ANP/INMETRO N$^o$ 1. 20.06.2011 - DOU - Diário Oficial da União, 2000.

Ansys, Inc. ANSYS CFX-Solver Theory Guide. Canonsburg, PA, USA, 2010a.

Ansys, Inc. ANSYS CFX$^{TM}$ Version 13.0. 2010b.

Carlander C. and Delsing J. Installation effects on an ultrasonic flow meter with implications for self diagnostics. *Flow Measurement and Instrumentation*, 11(2):109 – 122, 2000.

Ferreira A.L.A.S. *Tecnologia ultrassônica na medição de vazão em escoamentos incompressíveis*. D.Sc. Thesis, Pontifícia Universidade Católica do Rio de Janeiro, 2010.

Filho F.F.C. *Algoritmos Numéricos*. LTC, $2^{nd}$ edition, 2007.

Hilgenstock A. and Ernst R. Analysis of installation effects by means of computational fluid dynamics – CFD vs experiments? *Flow Measurement and Instrumentation*, 7(3-4):161 – 171, 1996.

Holm M., Stang J., and Delsing J. Simulation of flow meter calibration factors for various installation effects. *Measurement*, 15(4):235 – 244, 1995.

Köchner H., Melling A., and Baumgärtner M. Optical flow field investigations for design improvements of an ultrasonic gas meter. *Flow Measurement and Instrumentation*, 7(3-4):133

– 140, 1996.

Launder B.E. and Spalding D.B. The numerical computation of turbulent flows. *Computer Methods in Applied Mechanics and Engineering*, 3(2):269 – 289, 1974.

Martins R.S. and Ramos R. Numerical evaluation of upstream bend installation effects on fully developed flow profiles aiming ultrasonic flow metering. *Submitted to the 21$^{st}$ International Congress of Mechanical Engineering*, 2011a.

Martins R.S. and Ramos R. Uma abordagem numérica para o cálculo de fator de correção de medidores de vazão por ultrassom. *Submitted to the 6$^{o}$ Congresso Brasileiro de Pesquisa e Desenvolvimento em Petróleo e Gás*, 2011b.

Mathias R.B. *Influência do perfil de velocidade do escoamento sobre a medição ultra-sônica de vazão por tempo de trânsito*. Master's Thesis, Universidade Federal do Espírito Santo, 2010.

Mickan B., Wendt G., Kramer R., and Dopheide D. Systematic investigation of flow profiles in pipes and their effects on gas meter behaviour. *Measurement*, 22(1-2):1 – 14, 1997.

Moore P.I., Brown G.J., and Stimpson B.P. Ultrasonic transit-time flowmeters modelled with theoretical velocity profiles: methodology. *Measurement Science and Technology*, 11(12):1802, 2000.

Mylvaganam K. High-rangeability ultrasonic gas flowmeter for monitoring flare gas. *IEEE Transactions on Ultrasonics Ferroelectric and Frequecy Control*, 36(2):144 – 149, 1989.

Nikuradse J. Laws of turbulent flow in smooth pipes. NASA TT F-10, 359, National Aeronautics and Space Administration, Washington, USA, 1966. Translated from 'Gesetzmässigkeiten der turbulenten Strömung in glatten Rohern' Forsch. Arb. Ing.-Wes. No. 356 (1932).

Ruppel C. and Peters F. Effects of upstream installations on the reading of an ultrasonic flowmeter. *Flow Measurement and Instrumentation*, 15(3):167 – 177, 2004.

Schlichting H. *Boundary-Layer Theory*. McGraw-Hill series in Mechanical Engineering. McGraw-Hill, New York, USA, 6$^{th}$ edition, 1968.

Tennekes H. and Lumley J.L. *A First Course in Turbulence*. The MIT Press, Cambridge, Massachusetts, USA, 1972.

Versteeg H.K. and Malalasekera W. *An Introduction to Computational Fluid Dynamics - The Finite Volume Method*. Pearson Education Limited, Essex, England, 2007.

Yeh T.T. and Mattingly G.E. Computer simulations of ultrasonic flow meter performance in ideal and non-ideal pipeflows. In *ASME Fluids Engineering Division Summer Meeting - FEDSM'97*. ASME, 1997.